Available online at www.sciencedirect.com

ScienceDirect

Procedia Engineering 2 (2010) 1273–1281

Procedia Engineering

www.elsevier.com/locate/procedia

Fatigue 2010

Fatigue properties and crack propagation behavior of stainless cast steel for turbine runner of hydraulic power generation

Masahiko Natsume[a]*, Yoshiichirou Hayashi[b], Hiroyuki Akebono[a], Masahiko Kato[a], Atsushi Sugeta[a]

[a]*Hiroshima University, Higashihiroshima City, Japan*
[b]*Electric Power Development Co.,Ltd, Chigasaki City, Japan*

Received 4 March 2010; revised 11 March 2010; accepted 15 March 2010

Abstract

In order to clarify the fatigue properties of stainless cast steel JIS SCS6 used as the turbine runner of hydraulic power generation for about 27 years, fatigue tests were carried out by using tension-compression specimens , plane bending specimen and CT specimens. The results are summarized as follows: The fatigue strength of tension-compression was lower than that of plane bending. In order to examine the reason for that, fracture surfaces were observed by SEM. It is because that in the case of tension-compression fatigue tests, the increase of volume of dangerous layer which was applied high stress led the increase of the size of the casting defect included there for the loading mode and the shape of specimens. It suggests that casting defects strongly affect the fatigue properties of aging stainless cast steel. Furthermore, according to the estimation of fatigue life, it is clear that fatigue life of aged stainless cast steel can evaluate by using the casting defect size at crack initiation site and the stress intensity factor calculated by defect size. In addition, to clear the fatigue crack propagation behavior, the relationship between the fatigue crack growth rate and effective stress intensity range was examined by using the unloading elastic compliance method which can observe the detailed fatigue crack closure behavior.

keywords: Fatigue; fracture mechanism; stainless cast steel; crack behavior

1. Introduction

Hydraulic power generation is a power generation technology as important as thermal power and nuclear power generations. It has been paid to attention as a clean power generation technology with few carbon-dioxide emissions during power generation. One of the important components of such hydraulic power generation includes the turbine runner. In recent years, stainless cast steels, which has high strength and stiffness and excellent corrosion resistance and weldability compared with conventional cast steels are widely used for the turbine runner material [1]-[3]. However, there are a lot of turbine runners which passed more than several decades after manufacturing and some case that the turbine runner damaged by long-term use are reported. Therefore, appropriate maintenance method that enables long-term operation while maintaining the reliability of existing equipment is required because it needs huge

* Corresponding author. Tel.: +81-82-424-7538; fax: +81-82-424-7538.
E-mail address: m095750@hiroshima-u.ac.jp.

1877-7058
doi:10.1016/j.proeng.2010.03.138

cost to repair and replace the damaged turbine runner. It is necessary to understand the fatigue properties and the fracture mechanism of the turbine runner, in order to establish that maintenance method, although there are a few reports of the fatigue properties of the stainless cast steel[4][5]. Therefore, in this study, in order to clarify the fatigue properties of stainless cast steel for which several decades are used as the turbine runner of hydraulic power generation, three kinds of fatigue tests were carried out and fatigue crack behavior was observed in detail. In addition, the fatigue life prediction method of an actual power turbine runner was suggested in the bases of the obtained knowledge.

2. Specimens and experimental method

2.1. Specimen

The material used in this study was stainless cast steel JIS SCS6 (equivalent to ASTM CA6NM) used as the turbine runner of hydraulic power generation for about 27 years. Table 1 and Table 2 show the chemical composition and the mechanical properties of SCS6 respectively. This material was machined into three kinds of fatigue specimen shown in Fig.1 ((b) for plane bending fatigue tests, (a) for tension-compression fatigue tests, and (c) CT specimens). In addition, specimen for plane bending fatigue tests has an elliptic shallow notch (stress concentration factor K_t=1.26) at the center of it to localize a crack initiation site. The geometry of CT specimen follows ASTM standard. After machining into specimen, the specimen surfaces were polished using SiC paper (#180-#2000) and alumina powder (ϕ3.0μm, ϕ1.0μm, ϕ0.1μm).

Table1 Chemical composition of JIS SCS6. (mass%)

C	Si	Mn	P	S	Ni	Cr	N	Al	Ca	O
0.49	0.50	0.83	0.040	0.004	3.62	12.82	0.027	0.010	<0.0005	0.0063

Table2 Mechanical properties of JIS SCS6.

Vickers Hardness	Yield stress [MPa]	Tensile strength [MPa]
280	600	830

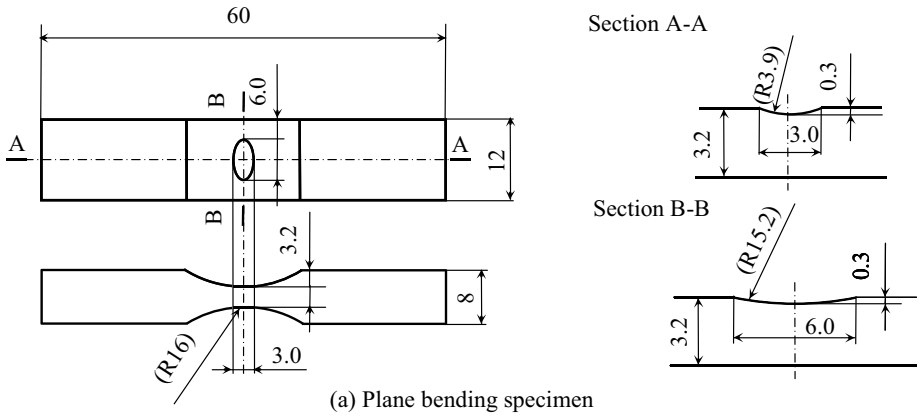

(a) Plane bending specimen

Fig.1 specimen geometry

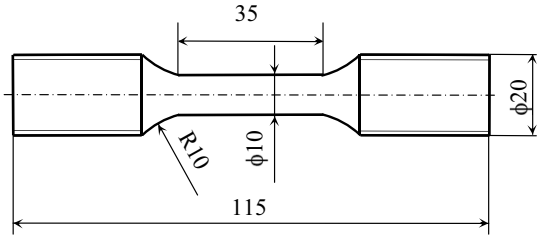

(b) Tension-compression specimen

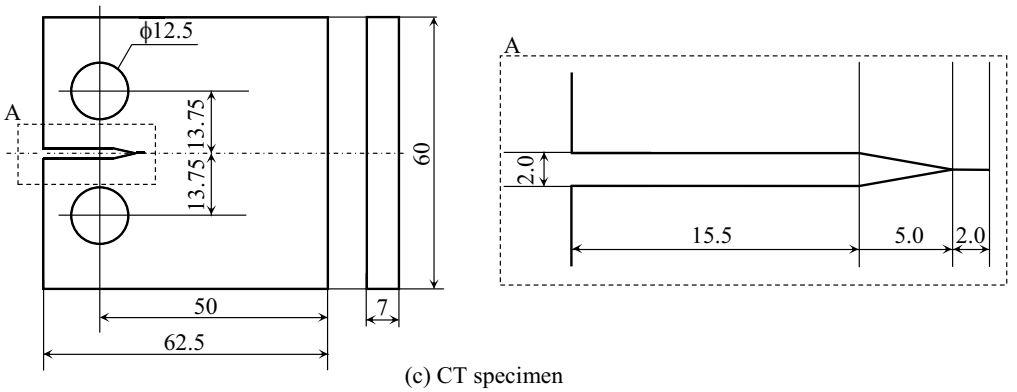

(c) CT specimen

Fig.1 continued

2.2. Experimental method

The tension-compression fatigue tests were carried out using a servo-hydraulic testing machine. The plane bending fatigue tests were carried out using an electro-magnetic type bending machine. The condition of fatigue tests were unified in both fatigue tests (sine wave load; frequency: 20 Hz; stress ratio: -1). Furthermore, in the case of bending fatigue tests, the small fatigue crack behavior was observed continuously by using a plastic replicas technique. The fatigue crack growth tests by using CT specimen were conducted using a servo-hydraulic testing machine as a frequency of 1~20 Hz and stress ratio R=0.05, $d\Delta K/(\Delta K \cdot da)$=0.1. Moreover, the crack length and the crack closure were measured by the unloading elastic compliance method [6]. Fracture surfaces were carefully observed under a Scanning Electron Microscope (SEM) to identify the fatigue crack initiation sites and the fracture mechanism.

3. Experimental results and discussion

3.1. Fatigue tests

Figure 2 shows the *S-N* curves. The vertical axis in this figure indicates the true stress amplitude in consideration of the notch in the case of specimens for plane bending fatigue tests. As shown in this figure, tension-compression fatigue test results indicate lower strength than plane bending fatigue test data. In order to examine the reason for that, fracture surfaces were observed by SEM. Figure 3 shows a typical fracture surface of tension-compression test.

It was observed that the fracture origin was the casting defect for this test. On the other hand, a lot of fracture origin was observed in a fracture surface for plane bending test in all stress range, there were two types of fracture origin. One of the fracture type whose fatigue crack initiation by slip deformation at surface and from the casting defects near the surface (Fig.4). Another is the fracture type whose fatigue cracks initiate by multiple slip deformation at surface only (Fig.5). As mention above, aging SCS6 used in this study has two types fatigue crack initiation mechanism; (a) *slip and defect origin type*, (b) *slip origin type*. Therefore, in Fig.2, open marks show the result which indicate *slip origin type*, and solid marks show the results which include *defect origin type*. It is clear that no noticeable variations exist in the *S-N* curves of specimens whose crack initiates at the slip. However, the *S-N* curves of specimens which indicate *slip and defect origin type* have wide variations, and the results using tension-compression fatigue tests indicate lower strength than that using plane bending fatigue tests. In order to examine the reason for that, the casting defect size which was fracture origin in each specimen was observed in detail.

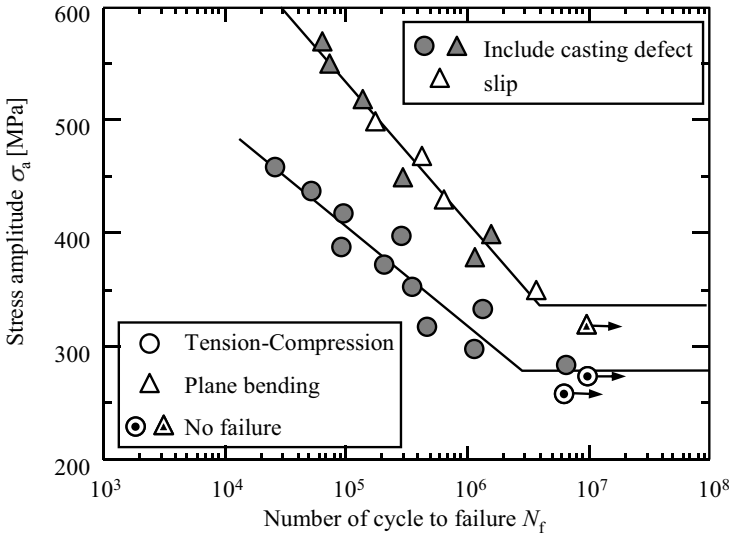

Fig.2 *S-N* curves

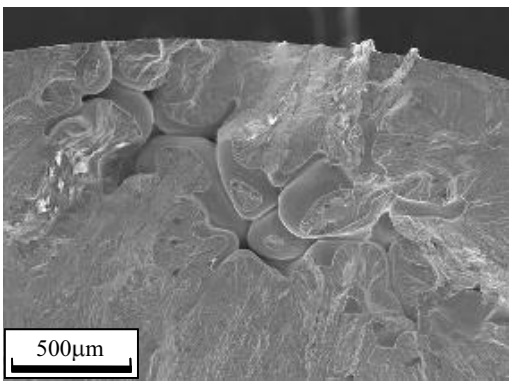

Fig.3 fracture origin of tension-compression test [σ_a=460MPa, N_f=2.6×10^4]

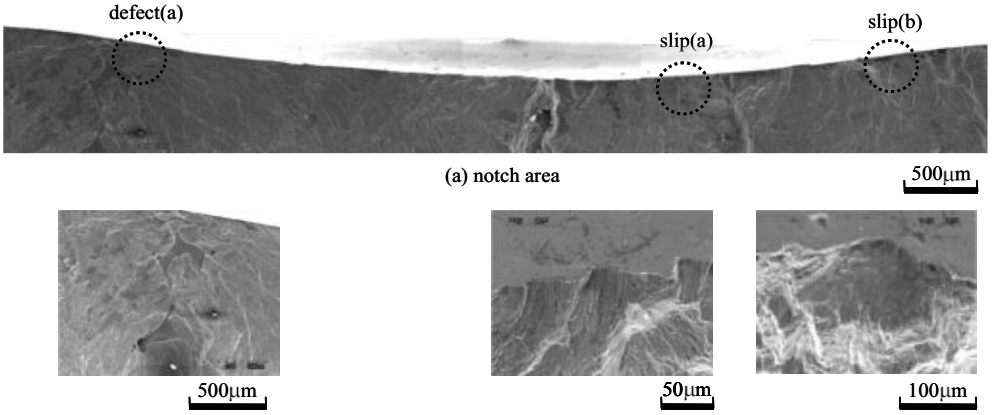

Fig.4 Fracture surface of plane bending test (slip and defect origin type) [380MPa,N_f=1.2×10^{6}cycles]

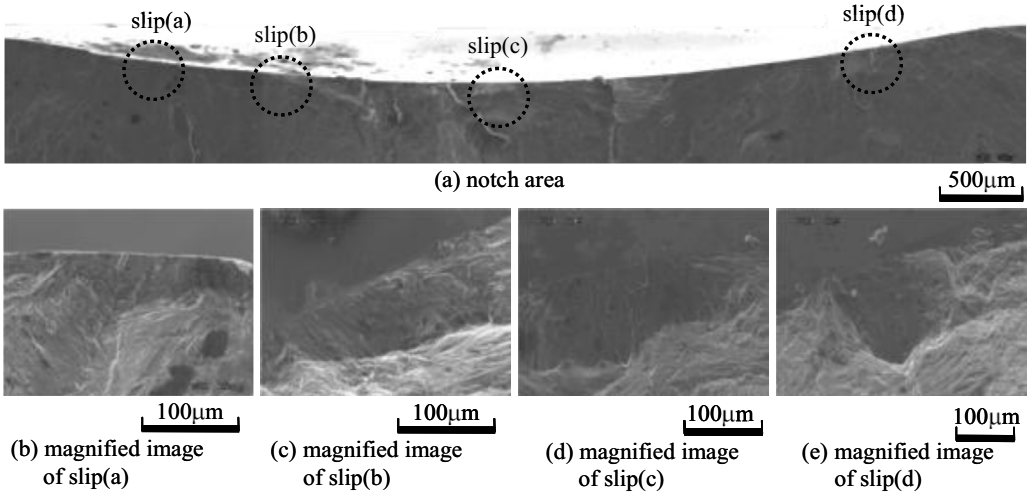

Fig.5 Fracture surface of plane bending test (slip origin type) [430MPa,N_f=6.6×10^{5}cycles]

The casting defect size $(area)^{1/2}$ are measured in each fractures surface in both tension-compression fatigue and plane bending fatigue tests, and plotted them in an external distribution (Fig.6). It is clarified that the casting defect size in aging SCS6 used in this study was well fitted by an external distribution. Furthermore, casting defect size of fracture origin in the specimens for tension-compression fatigue tests was larger than that for the plane bending fatigue tests. It is because that in the case of tension-compression fatigue tests, the increase of volume of dangerous layer which was applied high stress led the increase of the size of the casting defect included there for the loading mode and the shape of specimens. So, it can be thought factor that the increase of the casting defect size which is fracture origin led the decrease of the fatigue strength.

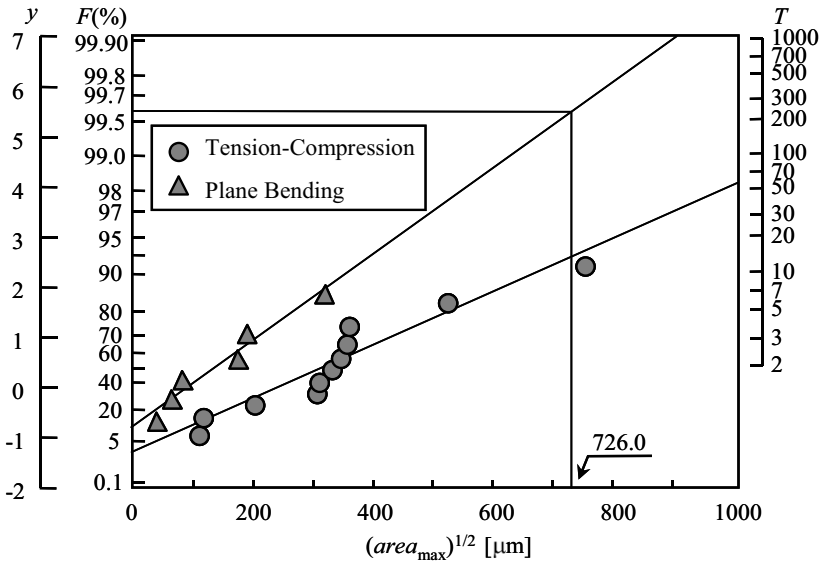

Fig.6 Distribution of defect size

From the results of fatigue tests and fracture surface observation mentioned above, it is clarified that the existence of casting defects and their size strongly affect the variation of fatigue strength in aging SCS6. So, *S-N* curve of this material was arranged in consideration of casting defects size which was fracture origin. Figure 7 shows the relationship between the initial stress intensity factor K_{max} which was calculate by equation (1),(2) in consideration of the casting defect size $(area)^{1/2}$ which were fracture origins in each specimen and $N_f/(area)^{1/2}$. In addition, K_{max} was calculated by equation (1) when the casting defect exists near the surface, by equation (2) when the casting defect exists internal far from the surface.

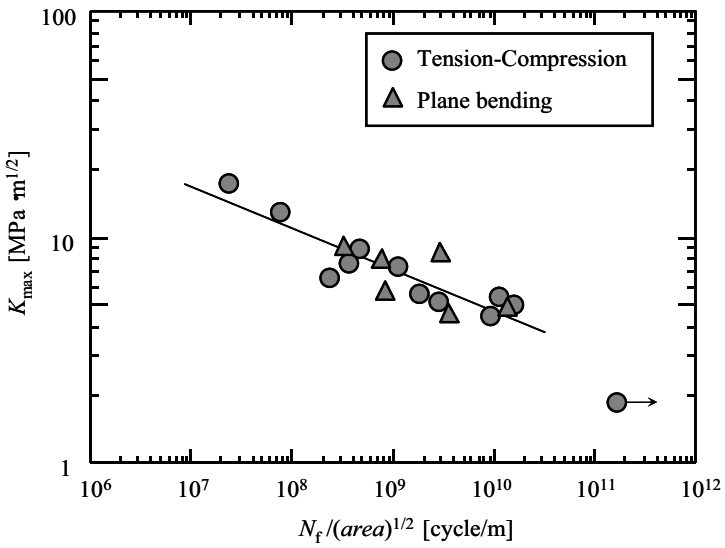

Fig.7 K_{max}-$N_f/(area)^{1/2}$ relationships

$$K_{\max} = 0.65\sigma\sqrt{\pi\sqrt{area}} \quad (1)$$

$$K_{\max} = 0.5\sigma\sqrt{\pi\sqrt{area}} \quad (2)$$

Figure 7 shows that it is possible to rearrange the fatigue life curve by evaluating casting defect size which was fracture origin and crack propagation life from their origins. Furthermore, it is possible to predict the fatigue life of aging SCS6 by using equation (3) which was led from approximate line in this figure.

$$N_{\mathrm{f}} = \left(\frac{K_{\max}}{317.5}\right)^{-5.46} \cdot \sqrt{area} \quad (3)$$

However, maximum defect size which will be in the actual turbine runner is required to apply the equation (3) to the actual turbine runner. So, in his section, we added discussions whether it is possible to predict the maximum defect size that will exist in a large structure from the defect size that exists in small specimen such as specimen for plane bending fatigue tests by using a statistics of extreme value. In the case of specimens for plane bending fatigue tests , the volume of dangerous layer which was applied stress of 90% or more was $V_{0.9\sigma,\mathrm{bending}}$=11.5[mm^3]. On the other hand, the volume of dangerous layer in specimens for tension-compression fatigue tests was V_{TC} =2747.5[mm^3]. Thus, the reflexive period $T_{0.9\sigma}$=239.5 can be obtained when the dangerous layer is defined as 90% of the loading stress. So, when we calculated the maximum defect size which will be exist in dangerous layer of specimens for tension-compression fatigue tests from the casting defect size of specimens for plane bending fatigue tests, the value of maximum defect size were $(area_{0.90\sigma})^{1/2}$=726.0[μm] as shown in Fig.6. Considering that the maximum defect size $(area_{\max})^{1/2}$ which was actually observed in fracture surface of specimens for tension-compression fatigue tests was 749.0[μm], it is clear that it is possible to predict the maximum defect size with high accuracy. However, we write in addition that a more detailed examination of defining method of a dangerous layer is necessary in the future.

3.2. Fatigue crack propagation behavior

Figure 8 shows the relationship between fatigue crack growth rate and stress intensity range ΔK, effective stress intensity rage ΔK_{eff}. This figure indicates linear relationship between da/dN and ΔK as show equation (4) (5).

$$\mathrm{d}a/\mathrm{d}N = 7\times10^{-12}(\Delta K)^{2.82} \quad (4)$$

$$\mathrm{d}a/\mathrm{d}N = 2\times10^{-12}(\Delta K_{\mathrm{eff}})^{2.97} \quad (5)$$

Furthermore, Fig.9 shows the relationship between the crack growth rate da/dN, which were observed in plane bending fatigue tests by replicas technique, and stress intensity factor ΔK_{nr} calculated by using Newman-Raju's equation. Small crack propagation behavior has particularly variation, so it shows a tendency that along long crack, and the propagation rate was similar to a long crack one.

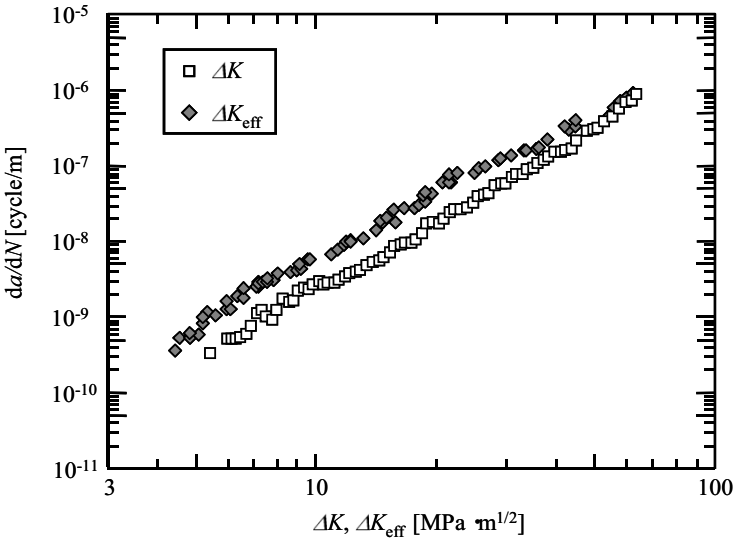

Fig.8 d*a*/d*N*- ΔK, ΔK_{eff}relationships

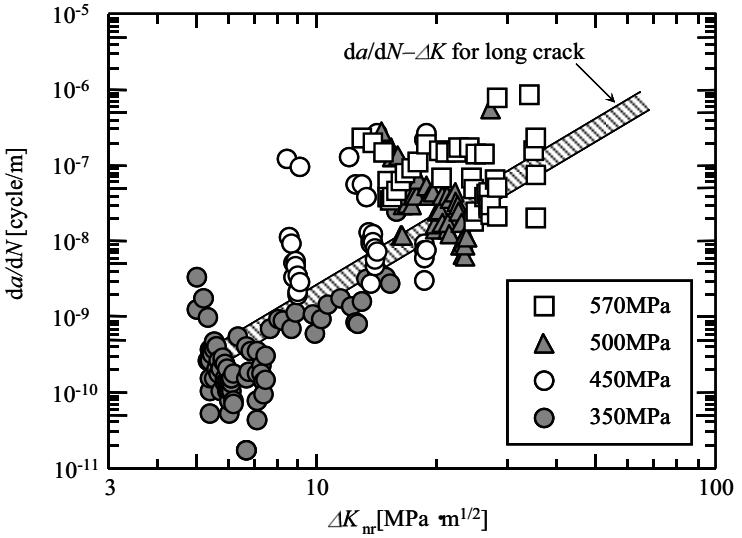

Fig.9 d*a*/d*N*- ΔK relationships of small crack

4. Conclusion

In order to clarify the fatigue properties of aging stainless cast steel JIS SCS6 for which several decades are used as turbine runner of the hydraulic power generation, three kinds of fatigue tests were carried out and fatigue crack behavior was observed in detail. Furthermore, the fatigue life prediction method of an actual power turbine runner was suggested base of the obtained knowledge. The following conclusion can be drawn.

(1) The S-N curve of aging JIS SCS6 used in this study indicates wide variation and the results using tension-compression fatigue tests show lower strength than that using plane bending fatigue tests.
(2) From the observation of fracture surface, the fatigue crack of this material initiated at two types crack initiation origin then the final fracture of specimen was occurred; *slip origin type* and *include defect origin type*.
(3) The fatigue life of JIS SCS6 can be predicted by using its casting defect size $(area)^{1/2}$ and the initial stress intensity range ΔK_{max} calculate there.
(4) Indicates linear relationship between the fatigue crack growth rate and the stress intensity range ΔK, effective stress intensity range ΔK_{eff} in the case of long fatigue crack. However, crack growth rate of small crack observed in plane bending fatigue tests has widely scatter.

References

[1] U.M. Dawoud, S.F. Vanweele, Z. Szklarska-Smialowska. The effect of H_2S on the crevice corrosion of aisi 410 and ca6nm stainless steels in 3.5% nacl solutions. *Corrosion Science*, Volume 33, Issue 2; 1992, p.295-306

[2] R. Chattopadhyay. High silt wear of hydroturbine runners. *Wear*, Volumes 162-164, Part 2; 1993, p.1040-1044

[3] Akhilesh K. Chauhan, D.B. Goel, S. Prakash. Solid particle erosion behavior of 13Cr–4Ni and 21Cr–4Ni–N steels. *Journal of Alloys and Compounds*, Volume 467, Issues 1-2; 2009, p. 459-464

[4] L.A. James, W.J. Mills. Fatigue-crack propagation and fracture toughness behavior of cast stainless steels. *Engineering Fracture Mechanics*, Volume 29, Issue 4; 1988, p. 423-434

[5] K.D. Bogie, D. Alexander, R. Kirk. Ageing of cast stainless steel components. International Journal of Pressure Vessels and Piping, Volume 50, Issues 1-3; 1992, p. 161-177

[6] Kikukawa, M., Nanbo, Jono, M., Tanaka, K., Takatan, M., Measurement of Fatigue Crack Propagation and rack.Closure at Low Stress Intensity level by Unloading Elastic Compliance Method, *Journal of the Society of Materials Science*, Vol.25, No.276(1976), pp.899-903